J|A|C|S COMMUNICATIONS

Published on Web 07/10/2009

Probing Ultrafast Internal Conversion through Conical Intersection via Time-Energy Map of Photoelectron Angular Anisotropy

Takuya Horio,[†,‡,§] Takao Fuji,[†,‡] Yoshi-Ichi Suzuki,[†,‡,§] and Toshinori Suzuki*[,†,‡,§]

CREST, Japan Science and Technology Agency, Sanbancho, Chiyoda-ku, Tokyo, 102-0075, Japan, Chemical Dynamics Laboratory, RIKEN Advanced Science Institute, Wako 351-0198, Japan, and Department of Chemistry, Graduate School of Science, Kyoto University, Kyoto 606-8502, Japan

Received June 11, 2009; E-mail: t-suzuki@riken.jp

In polyatomic molecules conical intersections (CIs)[1] of potential energy surfaces (PESs) efficiently funnel the nuclear motion on one adiabatic PES to another. Recent quantum mechanical calculations have unraveled the general importance of nonadiabatic dynamics through CIs in photochemical reactions and molecular functions, including the photostability of DNA bases against ultraviolet radiation. In this communication we present a novel approach for detecting nonadiabatic dynamics through CIs via the time-energy mapping of the photoelectron angular anisotropy.

Ultrafast electronic spectroscopy can track the motion of a nuclear wave packet by determining the time dependence of the spectral (energy or frequency) distribution.[1−3] However, the distribution is not necessarily sensitive to ultrafast changes in the electronic character. Although Seel and Domcke[3] have proposed the use of time-resolved photoelectron spectroscopy (TRPES) for real-time observation of the S_2 [$^1B_{2u}$ (π,π^*)] → S_1[$^1B_{3u}$ (n,π^*)] process in pyrazine, the best-known internal conversion through CIs, the TRPES performed by Stert et al. using 130 fs ultraviolet pulses[4] and its theoretical modeling by Hahn and Stock[5] revealed that the photoelectron kinetic energy distribution (PKED) does not change markedly upon internal conversion. This failure is attributed to the coincidence of the energy differences between S_2-D_1 (π^{-1}) and S_1-D_0 (n^{-1}) involved in the ionization process of pyrazine.

A more general and direct indicator of electronic character is the electronic transition dipole moment. In photoelectron spectroscopy, the transition dipole moment from a nonstationary state to the ionization continuum varies with nonadiabatic electronic transition, resulting in the variation of the photoelectron angular distribution (PAD).[6] However, it has also been noted that a photoelectron is ejected with a range of kinetic energy, and not all PADs at different PKEs are sensitive to nonadiabatic dynamics. In the present work, we employed time-resolved photoelectron imaging (TRPEI)[7,8] to visualize the time dependence of the PKED and PAD simultaneously with an unprecedented time resolution of 22 fs, and we clarified how internal conversion in this benchmark system can be detected by photoelectron imaging.

The 1 kHz pulse trains of the fundamental (800 nm, 25 fs, 0.5 mJ) and second harmonic (400 nm, 30 fs, 0.5 mJ) of a Ti:sapphire laser (KML, Dragon) were spatially and temporally overlapped and gently focused into a Ne gas cell (610 Torr). The self-focusing of these intense femtosecond laser pulses created multicolor filamentation through the gas, facilitating efficient nondegenerate four-wave mixing to produce 264 nm (4.70 eV) and 198 nm (6.26 eV) pulses.[9] These pulses were respectively shortened to 14 fs (264 nm) and 17 fs (198 nm) using a grating-based compressor. The cross-correlation of these pulses at the sample point was measured to be 22 fs by the nonresonant (1+1′) multiphoton ionization of ethanol. The time origin ($t = 0$) of the pump−probe time delay was determined accurately within a few femtoseconds, which enabled us to analyze the time profile accurately. The pump (264 nm) and probe (198 nm) pulses were focused onto a supersonic molecular beam of pyrazine seeded in He. The pulse energies were controlled to 0.5 μJ (264 nm) and 0.1 μJ (198 nm) to avoid saturation of the $S_2 \leftarrow S_0$ transition and one-color multiphoton ionization. The photoelectrons generated by the (1+1′) pump−probe photoionization were projected onto a two-dimensional (2D) position-sensitive detector, and 3D photoelectron velocity distributions were reconstructed from the images using the pBaseX method.[10]

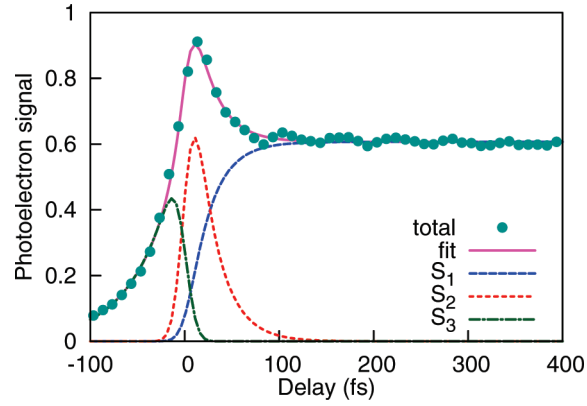

Figure 1. Temporal profile of total photoelectron signal in (1+1′) resonance enhanced multiphoton ionization (REMPI) of pyrazine via S_2($^1B_{2u}$). The observed data are consistent with single exponential decay from S_2 to S_1 for a positive time delay and single exponential decay of S_3 for a negative time delay.

Figure 1 shows the pump−probe photoelectron intensity as a function of time. The pump pulse is resonant with the $S_2 \leftarrow S_0$ transition near its origin, and the probe pulse spectrum slightly overlaps with $S_3 \leftarrow S_0$. Except for an oscillatory feature due to a vibrational quantum beat, the time profile is well explained by three components, i.e., rapid decay and a corresponding growth in the positive time range and decay in the negative time range. These respectively correspond to the decay of the optically excited S_2 (dotted line), the corresponding growth of S_1 (broken line) by internal conversion from S_2, and the decay of S_3 (dash-dotted line). The last component originates from the 198 nm pump and 264 nm probe process in the negative time range. From the least-squares fitting, we obtained the $S_2 \rightarrow S_1$ internal conversion time constant to be 23 ± 4 fs. Although the photoelectron signal in Figure 1 appears as a plateau within this time range, this long-lived

[†] CREST.
[‡] RIKEN.
[§] Kyoto University.

10.1021/ja904780b CCC: $40.75

component has a finite lifetime of ~22 ps (pyrazine-h4).[7] We performed a Fourier transform of the quantum beat and obtained its frequency to be 560 ± 40 cm^{-1}, from which it is assigned to the totally symmetric normal mode Q_{6a} in S_1 (583 cm^{-1}).[11]

We measured 2D photoelectron images for a number of pump−probe time delays and extracted the time dependence of the PKED (not shown here). However, we found that the PKED changes only slightly upon internal conversion in agreement with previous experimental and theoretical findings.[1,4,5] This is mainly because photoionization predominantly occurs as $D_0(n^{-1})$←$S_1(n,\pi^*)$ and $D_1(\pi^{-1})$←$S_2(\pi,\pi^*)$, in which the energy gaps between D_1-D_0 (0.88 eV) and between S_2-S_1 (0.86 eV) are almost the same.[12]

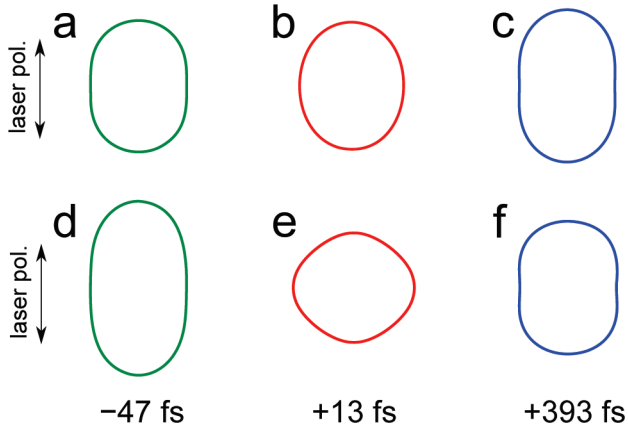

Figure 2. Polar plots of PADs observed for different time delays of (a) −47 fs, (b) +13 fs, and (c) +393 fs. The distributions are integrated for all PKE components. (d−f) PADs at the same time delays as (a−c), respectively, but with distributions of PKE of 0.8−0.9 eV. The time evolution is more evident in the selected-energy PADs shown in (d−f).

Now we direct our attention to the PAD. Figure 2 shows polar plots of PADs: (a−c) are the PADs integrated for all PKEs and (d−f) are those for PKE = 0.8−0.9 eV. Figure 2a and d, b and e, and c and f primarily correspond to PADs for the ionization from S_3, S_2, and S_1, respectively. Although a difference in the PADs is noticeable upon comparing (a−c), the difference is much clearer in plots (d−f); the PAD from S_2 shown in Figure 2e is horizontally elongated, which implies that an electron is ejected more toward the orthogonal direction to the laser polarization.

More quantitatively, in our experimental configuration with the linear and parallel polarization of the pump and probe laser beams, the PAD is expressed as follows:

$$I(E,\theta,t) = \frac{\sigma(E,t)}{4\pi}\{1 + \beta_2(E,t)P_2(\cos\theta) + \beta_4(E,t)P_4(\cos\theta)\}$$

where E, θ, and t are PKE, the electron ejection angle from the laser polarization direction, and the pump−probe time delay, respectively. $P_n(x)$ are nth order Legendre polynomials. $\sigma(E,t)$ describes the PKE distribution upon ionization. The great advantage of TRPEI is that it allows rapid and accurate measurements of $\beta_2(E,t)$ and $\beta_4(E,t)$. We have determined the 2D map of $\beta_2(E,t)$ as a function of PKE and time as shown in Figure 3. Positive (green-blue) and negative β_2 (orange) correspond to the preferential ejection of an electron parallel and perpendicular to the ionization laser polarization direction, respectively. A rapid change in β_2 is clearly identified within 30 fs at approximately PKE = 0.9 eV. Since a molecule cannot rotate within such an ultrashort time period (<50 fs), this change is solely attributed to the ultrafast evolution of the electronic character due to the S_2→S_1 internal conversion.

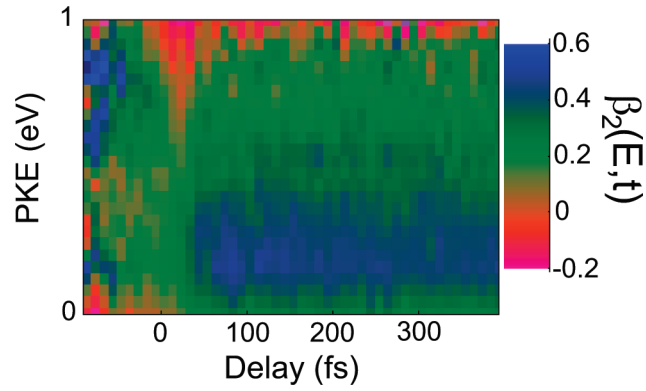

Figure 3. Photoelectron anisotropy parameter $\beta_2(E,t)$ determined for each time delay and PKE.

Note that PKE = 0.9 eV is not energetically allowed for the Koopmans type ionization process of $D_1(\pi^{-1})$← $S_2(\pi,\pi^*)$, and this component is unambiguously assigned to the non-Koopmans $D_0(n^{-1})$←S_2 process. In the PKE distribution, this non-Koopmans ionization signal is weaker than that for Koopmans type ionization; however, its negative β_2 is important for the real-time observation of the nonadiabatic transition in pyrazine. As can be seen in Figure 3, the Koopmans type ionization, $D_1(\pi^{-1})$ ← $S_2(\pi,\pi^*)$ and $D_0(n^{-1})$ ←S_1, creates a positive β_2, which is in agreement with our continuum multiple-scattering Xα calculations for pyrazine.

In conclusion, the time-energy mapping of the photoelectron anisotropy with an ultrahigh time resolution of 22 fs is a promising approach for studying the electronic character of a nonstationary state. We found that the non-Koopmans ionization process is the key to identifying the ultrafast internal conversion process in pyrazine.

Supporting Information Available: Details of pulse characterization and image analysis. This material is available free of charge via the Internet at http://pubs.acs.org.

References

(1) Domcke W., Yarkony D. R., Koppel H. *Conical Intersections, Vol. 15 of Advanced Series in Physical Chemistry*; World Scientific: Singapore, 2004.
(2) Werner, U.; Mitric, R.; Suzuki, T.; Bonacic-Koutecky, V. *Chem. Phys.* **2008**, *349*, 319–324.
(3) Seel, M.; Domcke, W. *J. Chem. Phys.* **1991**, *95*, 7806–7822.
(4) Stert, V.; Farmanara, P.; Radloff, W. *J. Chem. Phys.* **2000**, *112*, 4460–4464.
(5) Hahn, S.; Stock, G. *Phys. Chem. Chem. Phys.* **2001**, *3*, 2331–2336.
(6) Suzuki, Y.; Stener, M.; Seideman, T. *J. Chem. Phys.* **2003**, *118*, 4432–4443.
(7) Wang, L.; Kohguchi, H.; Suzuki, T. *Faraday Discuss.* **1999**, *113*, 37–46.
(8) Suzuki, T. *Annu. Rev. Phys. Chem.* **2006**, *57*, 555–592.
(9) Fuji, T.; Horio, T.; Suzuki, T. *Opt. Lett.* **2007**, *32*, 2481–2483.
(10) Garcia, G. A.; Nahon, L.; Powis, I. *Rev. Sci. Instrum.* **2004**, *75*, 4989–4996.
(11) Udagawa, Y.; Ito, M.; Suzuka, I. *Chem. Phys.* **1980**, *46*, 237–249.
(12) Oku, M.; Hou, Y.; Xing, X.; Reed, B.; Xu, H.; Chang, C.; Ng, C.-Y.; Nishizawa, K.; Ohshimo, K.; Suzuki, T. *J. Phys. Chem. A* **2008**, *112*, 2293–2310.

JA904780B